Fundamental Plasma Physics 7 (2023) 100026

Contents lists available at ScienceDirect

Fundamental Plasma Physics

journal homepage: www.elsevier.com/locate/fpp

Original research article

Symmetric Compton Scattering: A way towards plasma heating and tunable mono-chromatic gamma-rays

L. Serafini [a,b], A. Bacci [a,b], C. Curatolo [a,b], I. Drebot [a,b], V. Petrillo [a,c], A. Puppin [a,c], M. Rossetti Conti [a,b,*], S. Samsam [a,b]

[a] INFN-Section of Milan, Via G. Celoria 16, Milan, 20133, Italy
[b] INFN-LASA, Via F. Cervi 201, Segrate, 20090, Italy
[c] University of Milan, Via G. Celoria 16, Milan, 20133, Italy

ARTICLE INFO

Keywords:
Compton Scattering
Electron beam
Magnetic confinement
Gamma-ray source

ABSTRACT

This paper explores the transition between Compton Scattering and Inverse Compton Scattering (ICS), which is characterized by an equal exchange of energy and momentum between the colliding particles (electrons and photons). This regime has been called Symmetric Compton Scattering (SCS) and has the unique property of eliminating the energy-angle correlation of scattered photons, and, when the electron recoil is large, transferring monochromaticity from one colliding beam to the other, resulting in back-scattered photon beams that are intrinsically monochromatic. The paper suggests that large-recoil SCS or quasi-SCS can be used to design compact intrinsic monochromatic γ-ray sources based on compact linacs, thus avoiding the use of GeV-class electron beams together with powerful laser/optical systems as those typically required for ICS sources. Furthermore, at low recoil and low energy collisions (in the 10 keV energy range), SCS can be exploited to heat the colliding electron beam, which is widely scattered with large transverse momenta over the entire solid angle, offering a technique to trap electrons into magnetic bottles for plasma heating.

1. Introduction

The spectral red-shift observed when an X-ray pulse interacts with a carbon target was observed by Arthur Compton in 1922 Ref. [1] and interpreted as an effect of the collision between the photons of the X-rays and the electrons of the solid, both assumed as point-like particles. The scattering of the energetic photons by the electrons at rest in the laboratory was called (direct) Compton effect after him.

In more recent years, the Inverse Compton Scattering (ICS) effect was studied [2] and experimentally demonstrated in pivotal experiments at particle accelerators [3], using highly relativistic electrons colliding with laser beams, within an inverse kinematics set-up where the electron loses energy and momentum in favor of the incident photon, that is back-scattered and up-shifted to much larger energies. Compton sources are devices that have been developed and are currently in operation in many laboratories [4–13] with plenty of applications. Details about these facilities can be found in Ref. [14] While the Compton (both direct and inverse) effect cannot be explained classically, the low recoil regime of ICS, in which the electron energy/momentum loss is negligible, has been described in the framework of classical electrodynamics and it is known as Thomson effect Ref. [15]. In this paper, we analyze the transition from direct Compton (DC) to ICS, occurring when the colliding particles exchange an equal amount of energy and momentum, and we call this regime Symmetric Compton Scattering (SCS). In this particular condition, the properties of the scattered photons are unique: unlike in all other radiations emitted with a Lorentz boost, SCS scattered photon energy indeed no longer depends on the scattering angle, so that the back-scattered radiation beam becomes intrinsically monochromatic. Extending the analyses on large electron recoil ICS carried out in Refs. [16,17] to this particular regime, we find that SCS is characterized by the transfer of monochromaticity from one colliding beam to the other, so that when a large bandwidth photon beam collides under SCS conditions with a monoenergetic electron beam, the back-scattered photon beam results to be monochromatized. The possible applications range in many fields. SCS or quasi-SCS at large recoil could allow for the design of compact sources of intrinsic monochromatic γ-rays supplied by low energy MeV electron bunches, thus avoiding the use of GeV-class accelerators and powerful laser/optical systems, ac-

* Corresponding author.
E-mail address: marcello.rossetti@mi.infn.it (M. Rossetti Conti).

https://doi.org/10.1016/j.fpp.2023.100026
Received 11 July 2023; Received in revised form 18 September 2023; Accepted 3 October 2023
Available online 6 October 2023

tually needed by ICS sources. On the other hand, the SCS effect at low recoil can provide an electron heater based on X-rays. The scheme of the paper is the following. Section 2 will provide an overview of the various Compton interaction regimes between electrons and photons, focusing on the characteristics of the involved relativistic kinematics relevant to assess the collective properties of the secondary beams generated in the collision. Section 3 will present formulations of these regimes using four-vectors, to underline the behavior of the available energy in the center of mass reference system. Section 4 will focus on the dependence of secondary beam characteristics at large recoil regimes in high energy Compton scattering. In addition, section 5 will showcase simulations focusing on the SCS and quasi-SCS regime. Section 6 will discuss a mechanism for heating up an electron beam using SCS, useful to trap effectively electrons into a magnetic bottle (MB). Section 7 will present the conclusions discussing a practical application.

2. Compton interaction regimes

Considering the Compton interaction between photon pulses and counter-propagating electrons, we can derive the well-known equation for the photon energy ($E'_{\rm ph} = \hbar\omega'$, with ω' being the photon angular frequency and $\hbar$ the reduced Planck constant) scattered at an angle θ. Following the notation of Eq. 3 in Ref. [18], we can write:

$$E'_{\rm ph}(\theta) = \frac{(1+\beta)\gamma^2}{\gamma^2(1-\beta\cos\theta) + \frac{X}{4}(1+\cos\theta)} E_{\rm ph}, \tag{1}$$

where the incident photon energy is $E_{\rm ph} = \hbar\omega$, $\beta = v_e/c$ is the dimensionless electron velocity v_e (c being the speed of light), $\gamma = 1/\sqrt{1-\beta^2}$ is electron Lorentz factor and X is the electron recoil factor that introduces an important contribution at high energy of both incident photons and electrons. X has been defined in [17] (eq. 4) as:

$$X = \frac{4E_e E_{\rm ph}}{(m_0c^2)^2} = \frac{4\gamma E_{\rm ph}}{m_0c^2} = 4\gamma^2\frac{E_{\rm ph}}{E_e}, \tag{2}$$

with m_0 the electron rest mass and $E_e = \gamma m_0 c^2$. Eq. (1) can be cast in a more schematic form as a function of the incident particle energies.

$$E'_{\rm ph} = \frac{(1+\beta)\,E_{\rm ph}E_e}{(1-\beta\cos\theta)\,E_e + (1+\cos\theta)\,E_{\rm ph}}$$

The differential cross section, denoted as $d\sigma/d\Omega$, where Ω represents the solid angle $\sin\theta d\theta d\phi$ (with θ and ϕ being the zenithal and azimuthal angles of the momentum, respectively), is described by the Klein-Nishina formula:

$$\frac{d\sigma}{d\Omega} = \frac{r_e^2}{4\gamma^2(1+\beta)}\left(\frac{E'_{\rm ph}}{E_{\rm ph}}\right)^2\Psi, \tag{3}$$

with Ψ given by

$$\Psi = \frac{X^2}{16\gamma^4}\frac{(1+\cos\theta)^2}{(1-\beta\cos\theta)(1+\beta)}\frac{E'_{\rm ph}}{E_{\rm ph}} + 4\left(\mathbf{q}\cdot\mathbf{q}'\right) \tag{4}$$

where $\mathbf{q}$ and $\mathbf{q}'$ are the polarization versors of the incoming and outcoming photons, respectively and r_e is the classical electron radius. As can be seen, the differential cross section presents two terms, one proportional to the square of the recoil factor, the other containing the polarization. The total cross section can be obtained by integrating over θ and ϕ, and summing over all the polarizations:

$$\sigma = \frac{4\pi r_e}{X(1+\beta)}\left[\frac{1}{2} + \frac{16}{X(1+\beta)} - \frac{1}{2+X(1+\beta)} + \right.$$
$$\left. + \left(1 - \frac{8}{X(1+\beta)} - \frac{32}{X^2(1+\beta)^2}\right)\log\left(1+\frac{X}{2}(1+\beta)\right)\right]. \tag{5}$$

We can distinguish the following different interaction regimes: Direct, Inverse and Symmetric Compton Scattering.

2.1. Direct Compton

The collision between high energy photons and electrons at rest ($E_{\rm ph} \gg T_e$, where $T_e = (\gamma-1)m_0c^2$) is usually called Direct Compton (DC) scattering. In this process, the photon loses energy, being redshifted, while the collided electron gains energy, being recoiled.

The interaction studied in Arthur Compton's original experiment exploited X-rays incident on a fixed target ($\beta = 0$, $\gamma = 1$). Eq. (1) reduces to:

$$E'_{\rm ph}(\theta) = \frac{E_{\rm ph}}{1 + \frac{X_{DC}}{4}(1+\cos\theta)}. \tag{6}$$

In this case, the electron recoil factor can be rewritten as a function of the well-known electron Compton wavelength $\lambda_C = h/(m_0c)$ and the colliding photon wavelength λ:

$$X_{DC} = \frac{4E_{\rm ph}}{m_0c^2} = \frac{4\lambda_C}{\lambda}, \tag{7}$$

where $\lambda = hc/E_{\rm ph}$, leading directly to Compton's relationship for the scattered photon wavelength λ':

$$\lambda' - \lambda = \lambda_C(1+\cos\theta). \tag{8}$$

The redshift in photon wavelength allowed Arthur Compton to invoke the quantum nature of the photon-electron collision for explaining the experimental data. Moreover, the formula evidently shows the characteristic signature of radiation emission in collisions, i.e., the angular dependence of the scattered photon energy.

The differential cross section for this process is given by:

$$\frac{d\sigma}{d\Omega} = \frac{r_e^2}{4}\left(\frac{E'_{\rm ph}}{E_{\rm ph}}\right)^2\Psi, \tag{9}$$

with Ψ given by

$$\Psi = \frac{{X_{DC}}^2}{16}(1+\cos\theta)^2\frac{E'_{\rm ph}}{E_{\rm ph}} + 4(\mathbf{q}\cdot\mathbf{q}'), \tag{10}$$

while the total cross section, adding all the polarizations, becomes:

$$\sigma = \frac{4\pi r_e}{X_{DC}}\left[\frac{1}{2} + \frac{16}{X_{DC}} - \frac{1}{2+X_{DC}} + \right.$$
$$\left. + \left(1 - \frac{8}{X_{DC}} - \frac{32}{{X_{DC}}^2}\right)\log\left(1+\frac{X_{DC}}{2}\right)\right]. \tag{11}$$

The original Compton experiment was performed with hard X-rays of about 17 keV, so that X_{DC} was about 3 10^{-2} and the terms weighted by the recoil factor can be disregarded. The total cross section is, therefore, close to the Thomson value:

$$\sigma = \sigma_T\left(1 - \frac{X_{DC}}{2}\right), \tag{12}$$

where $\sigma_T = 6.65\ 10^{-29}$ m^2 is the Thomson cross section. The angular distribution, moreover, is approximately given by the Thomson expression:

$$\frac{d\sigma}{d\theta} = \frac{3}{8}\sigma_T\left(1+\cos^2\theta\right)\sin\theta. \tag{13}$$

2.2. Inverse Compton Scattering

The Inverse Compton Scattering (ICS) regime is instead characterized by collisions of highly energetic electrons and low energy photons (in most cases delivered by lasers) with $E_{\rm ph} \ll T_e$. In this interaction, the photon acquires energy from the electron. ICS sources are characterized by high electron beam energies (ranging from tens to hundreds of MeV), i.e. $\beta \to 1$ and $\gamma \gg 1$. Except for few interesting studies [16,17], the recoil factor in Compton devices does not exceed the value 10^{-2}. In

these conditions, due to the Lorentz boost effect, most of the emitted radiation is concentrated in a cone with rms angular aperture of the order of γ^{-1}. For θ small, $cos(\theta) \approx 1 - \theta^2/2$ and Eq. (1) can be approximated with:

$$E'_{\rm ph}(\theta) = \frac{4E_{\rm ph}\gamma^2}{1 + X + \gamma^2\theta^2}. \tag{14}$$

Equations (1) and (6) show the intrinsic dependence of the scattered photon energy on the scattering angle through the term $\theta\gamma$ in the denominator.

The maximum photon energy is achieved by fully back-scattered photons along the axis, at $\theta = 0$: $E'_{\rm ph}(\theta = 0) = 4E_{\rm ph}\gamma^2/(1 + X)$. In the case of negligible recoil, as in the Thomson regime, the maximum photon energy just reduces to $E'_{\rm ph}(\theta = 0) = 4E_{\rm ph}\gamma^2$. In the deep recoil regime, i.e. when $X \gg 1$, the maximum photon energy value is found on axis and is close to the electron energy

$$E'_{\rm ph}(\theta = 0) = \left(1 - \frac{1}{X}\right) E_e. \tag{15}$$

Eq. (15) shows that, in deep recoil, the scattered photon acquires the whole energy available in the collision, mostly carried by the incident electron. The electron almost stops after the collision while releasing its entire kinetic energy to the scattered photon. The electron-photon interaction in deep recoil scatters back the photon with an energy approaching the initial electron energy, with slight corrections due to the scattering angle and to the recoil factor.

2.3. Symmetric Compton Scattering

We refer to the regime of transition between DC and ICS as Symmetric Compton Scattering (SCS), where the energy/momentum transfer between photons and electrons is balanced. The maximum photon energy closely approaches the electron energy. Referring to equation 1, the dependence on θ of $E'_{\rm ph}$ cancels when:

$$\frac{X}{4} = \beta\gamma^2, \tag{16}$$

a condition valid when the photon and electron energies satisfy the relation $E_{\rm ph} = \beta E_e$, corresponding to equal electron and photon momenta with opposite directions $\vec{p}_e = -\vec{p}_{\rm ph}$. In this peculiar situation, the following relation exists between the electron kinetic energy $T_e = E_e - m_0c^2$ and the incident photon energy:

$$E_{\rm ph} = m_0c^2\sqrt{\frac{2T_e}{m_0c^2} + \left(\frac{T_e}{m_0c^2}\right)^2}.$$

Moreover, we can introduce an asymmetry factor

$$A = \beta\gamma^2 - \frac{X}{4} \tag{17}$$

that vanishes ($A = 0$) in SCS regime, assumes large positive values ($A \to \gamma^2$) in ICS regime (that is indeed characterized by $X \ll 4\beta\gamma^2$) and negative values in DC when $\beta = 0$. It is worth noting that the condition $A = 0$ indeed deletes the angular dependence shown in Eq. (1).

In the SCS regime, the center of mass of the collisions is at rest in the laboratory reference frame (see next chapter), therefore the produced radiation is not Lorentz transformed and its frequency is not boosted. As a result, the energy of the scattered photons is:

$$E'_{\rm ph} = E_{\rm ph}\ \forall\theta. \tag{18}$$

For convenience, we call E'_0 the value that Eq. (1) assumes for $\theta = 0$:

$$E'_0 = E'_{\rm ph}(\theta = 0) = \frac{2\gamma^2(1 + \beta)}{2\gamma^2(1 - \beta) + X} E_{\rm ph}. \tag{19}$$

Expressing Eq. (1) in Taylor Expansion of θ around $\theta = 0$ we find the following first two terms:

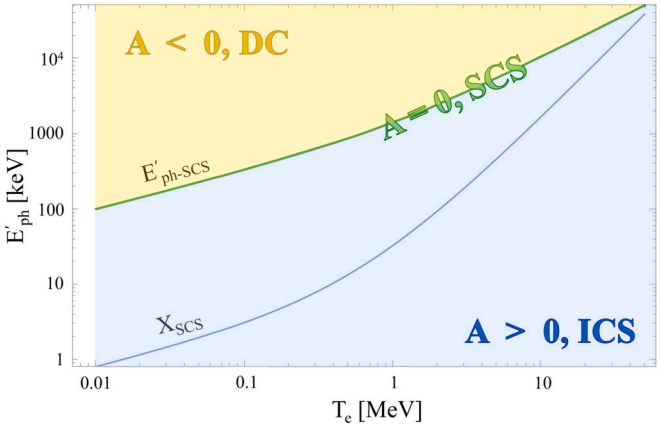

Fig. 1. Evolution of the recoil factor X value and of the scattered photon energy in SCS regime as a function of the electron kinetic energy T_e. Colored areas identify the possible Compton Scattering regimes and the relative asymmetry factor A sign, DC in yellow ($A < 0$), ICS in blue ($A > 0$) and in green the SCS divide line ($A = 0$).

$$E'_{\rm ph}(\theta) = E'_0 - \frac{E'_0}{\gamma^2}\frac{A\gamma^2\theta^2}{2\gamma^2(1 - \beta) + X} + A\ O(\gamma^4\theta^4), \tag{20}$$

where the higher order terms confirm that the symmetry condition ($A = 0$) cancels the angular correlation.

Note that the asymmetry factor A is negative in DC regime, where $\beta = 0$ and $\gamma = 1$, and $A = -\lambda_C/\lambda$. On the other side, in ICS regime the asymmetry factor A is positive and scales like γ^2. Equation (20) is actually a generalization of a well-known formula in ICS, that reads $dE'_{\rm ph}/E'_0 = \gamma^2\theta^2/(1 + X)$. Fig. 1 and 2 show the dependence of E'_0 vs. T_e and of the recoil factor X in different regimes (DC, SCS, ICS), that are associated with the sign of the asymmetry factor A.

It is interesting to derive the first order variation of the photon and electron energies after scattering as a function of the asymmetry factor A around SCS ideal conditions at A = 0. For that, we assume that A is given by a small quantity parameter δ_A, as $A = \delta_A \ll 1$, so that $X/4 = \beta\gamma^2 - \delta_A$ (see Eq. (16) and (17)). If $E_e = \gamma mc^2$ is the energy of the incident electron, then the energy of the incident photon will be given by $E_{\rm ph} = \beta E_e - \delta_A mc^2/\gamma$. Developing Eq. (1) up to first order in the small quantity δ_A we derive the energies $E'_{\rm ph}$ and $E'_{\rm e}$ of the photon and electron after scattering.

$$\begin{aligned} E'_{\rm ph} &= E_{\rm ph}\left(1 + \frac{\delta_A(1 + \cos\theta)}{(1 + \beta)\gamma^2}\right) \\ E'_e &= E_e - E_{\rm ph}\delta_A\frac{1 + \cos\theta}{(1 + \beta)\gamma^2}. \end{aligned} \tag{21}$$

Recalling that $\delta_A > 0$ means I.C.S., while $\delta_A < 0$ implies D.C., we just check that when $\delta_A = 0$, i.e. in ideal SCS conditions, we have (in agreement with Eq. (18))

$$\begin{cases} E_{\rm ph} = \beta E_e \\ E'_{\rm ph} = E_{\rm ph} \\ E'_e = E_e \end{cases} \tag{22}$$

i.e. the energies of electron and photon do not change before and after SCS, which is another unique characteristic of Symmetric Compton Scattering, that does not occur in any other electron-photon collision. This is represented by the $A = 0$ line plotted in Fig. 1.

Fig. 2 instead displays the dependence of the recoil factor X as a function of both the kinetic energy of the colliding electron T_e and the energy of the incident photon $E_{\rm ph}$. It is well visible that in order to achieve very large recoil factors, say of the order of one thousand, the electron energy and the photon energy must be both larger than about 10 MeV. The line marked $X_{\rm SCS}$ shows the recoil factor value in SCS conditions, i.e. when $E_{\rm ph} = \beta E_e$, or $A = 0$.

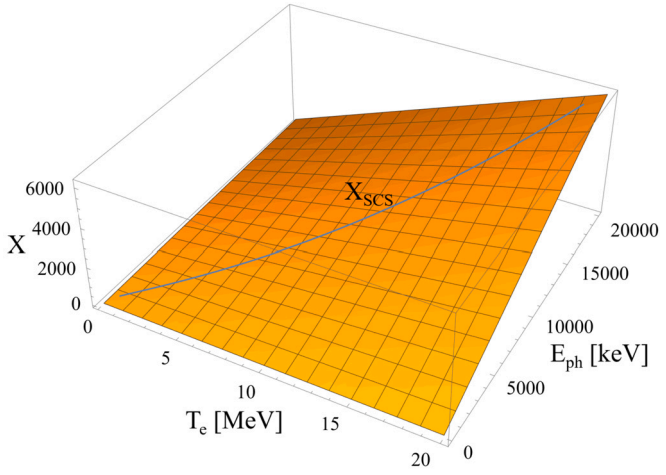

Fig. 2. 3D representation of the value of the recoil factor X as a function of the interacting electron kinetic energy T_e and of the incident photon energy $E_{\rm ph}$. The line shows the recoil value in SCS conditions.

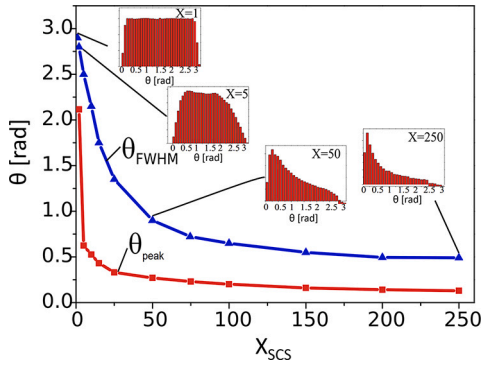

Fig. 3. Photon angular distribution in Symmetric Compton Scattering for different values of recoil factor X_{SCS} in the unpolarized case. The figure represents the peak value of the distribution of the zenithal momentum angle θ_{peak} (in red) and the full width half maximum θ_{FWHM}. The inner windows show the photon distribution shape for $X_{SCS} = 1, 5, 50$ and 250.

The differential cross section in this case becomes:

$$\frac{d\sigma}{d\Omega} = \frac{r_e^2}{4\gamma^2(1+\beta)}\left(\frac{(1+\cos\theta)^2\beta^2}{(1-\beta\cos\theta)(1+\beta)} + 4(\mathbf{q}\cdot\mathbf{q}')\right). \tag{23}$$

The symmetry condition can be satisfied in a regime of low or large recoil, depending substantially on the electron's energy. When $X \leq 1$, namely when $\gamma \leq 1.03$ or $\beta < 0.24$, the term of the angular cross section weighted by the recoil factor, proportional to β^2, is negligible and the angular distribution of photons and electrons after the scattering is almost flat, with the scattered particles spread on the whole solid angle. When the recoil is strong ($X_{SCS} \gg 1$), corresponding to β close to 1 and larger Lorentz factor, the angular distribution of photons and electrons in eq. (24) is determined by the term of the cross section proportional to β^2, with the angular dependence strongly peaked close to $\theta = 0$.

$$\frac{d\sigma}{d\Omega} = \frac{r_e^2}{4\gamma^2(1+\beta)^2}\frac{(1+\cos\theta)^2\beta^2}{(1-\beta\cos\theta)} \simeq \frac{r_e^2}{16\gamma^2}\frac{(1+\cos\theta)^2}{(1-\beta\cos\theta)}. \tag{24}$$

Fig. 3 illustrates the variation in the angular distribution of photons as a function of the recoil factor X_{SCS}. In the figure, the peak value of the zenithal angle distribution $\theta_{\rm peak}$ (in red) and the full width half maximum θ_{FWHM} (in blue) vs X_{SCS} are represented. The inner windows display the photon distribution shape for $X_{SCS} = 1, 5, 50$ and 250. When $X_{SCS} \leq 1$, the distribution is completely flat, the average value of the zenithal angle about $\pi/2$, its full width half maximum is close to π, and the rms just lower than $\pi/\sqrt{12}$. Increasing X_{SCS}, the distribution develops a peak on the side of lower angles, which is more and more pronounced and a tail towards the large angle. The rms value remains attained to about 0.75, but the full width half maximum decreases substantially, showing features connected to the dominant term in the cross-section when $X_{SCS} \gg 1$. The distribution of the scattered electrons appears to be similar to that of photons but rotated towards $\theta = \pi$.

3. A four-vector description

The four-momentum of a particle is defined as $\mathbf{p} = \left(\frac{E}{c}, p_x, p_y, p_z\right)$, where E is the total energy of the particle, c is the speed of light in vacuum, and p_x, p_y, p_z are the components of the particle's momentum along the x, y, z axes respectively.

Let us consider the case of a head-on collision between a photon and a counter-propagating electron along the z-axis. Before the collision, the electron and the photon have the following four-momenta:

$$\begin{aligned}\mathbf{p_e} &= \left(\gamma m_0 c, 0, 0, \beta\gamma m_0 c\right),\\ \mathbf{p_{ph}} &= \left(\tfrac{E_{\rm ph}}{c}, 0, 0, -\tfrac{E_{\rm ph}}{c}\right),\end{aligned} \tag{25}$$

and the total four-momentum is:

$$\mathbf{p_{tot}} = \left(\gamma m_0 c + \frac{E_{\rm ph}}{c}, 0, 0, \beta\gamma m_0 c - \frac{E_{\rm ph}}{c}\right). \tag{26}$$

The energy available in the center of mass E_{cm}, in terms of the recoil factor introduced in Eq. (2), is:

$$\begin{aligned}E_{cm} = c\sqrt{\mathbf{p_{tot}}\cdot\mathbf{p_{tot}}} &= m_0c^2\sqrt{(1+\beta)\frac{X}{2}+1} = \\ &= m_0c^2\sqrt{(1+\beta)\frac{2E_eE_{\rm ph}}{(m_0c^2)^2}+1}.\end{aligned} \tag{27}$$

The different regimes of Compton scattering can be analyzed in terms of their center of mass energy E_{cm}.

For the DC regime ($\beta = 0$, $\gamma = 1$):

$$E_{cm-DC} = m_0c^2\sqrt{\frac{2E_{\rm ph}}{m_0c^2}+1}. \tag{28}$$

On the opposite side, in the ICS regime ($\beta \simeq 1$), we obtain:

$$E_{cm-ICS} = m_0c^2\sqrt{X+1} = m_0c^2\sqrt{\frac{4\gamma E_{\rm ph}}{m_0c^2}+1}. \tag{29}$$

Finally, for the SCS regime ($E_{\rm ph} = \beta E_e = \beta\gamma m_0c^2$):

$$E_{cm-SCS} = (1+\beta)\gamma m_0c^2. \tag{30}$$

In this peculiar situation, $E_{cm} \propto \gamma$ like in a collider. Being $\gamma_{cm} \equiv E_{lab}/E_{cm}$ the Lorentz boost factor associated to the center of mass reference frame. In SCS we have $\gamma_{cm} = 1$ (because $E_{lab-SCS} = E_{cm-SCS}$), meaning that the center of mass of the system is at rest in the laboratory system, and the radiation produced here has the same angular and spectral distribution seen by a detector at rest in the lab. On the other hand, DC and ICS exhibit a dependence of the available energy E_{cm} typical of a fixed target collision, where E_{cm} scales like $E_{cm} \propto \sqrt{T_p}$, where T_p is the projectile kinetic energy. ICS regime is characterized by $\gamma_{cm} \gg 1$ since the center of mass reference frame is almost traveling with the electron (as shown in Ref. [17] $\gamma_{cm} = \gamma/(1+X)$).

4. Effects of deep recoil in Compton scattering

The energy spread of the scattered photon beam ($dE'_{\rm ph}/E'_{\rm ph}$, that is typically referred to as relative bandwidth) has a vanishing dependence on the energy spread of the incident photon beam ($dE_{\rm ph}/E_{\rm ph}$) whenever the recoil factor is very large. This effect is clearly illustrated in Ref. [18], Eq. 9 for the Compton scattering interaction:

$$\frac{dE'_{ph}}{E'_{ph}} = \frac{2+X}{1+X}\frac{d\gamma}{\gamma} + \frac{1}{1+X}\frac{dE_{ph}}{E_{ph}} \tag{31}$$

In this equation, the impact of high recoil factor values of X can be seen in the form of damping of the dependence of energy spread for the scattered photon beam ($\frac{dE'_{ph}}{E'_{ph}}$) on the energy spread of the incident photon beam ($\frac{dE_{ph}}{E_{ph}}$) and a result that's equal to the energy spread of the incident electrons ($\frac{d\gamma}{\gamma}$).

We derive the dependence of the outgoing photon energy spread on the incident photon energy spread to study the effect of deep recoil:

$$\frac{dE'_0}{E'_0} = \frac{\frac{2}{1+\beta}}{2(1-\beta)\gamma^2 + X}\frac{dE_0}{E_0} = \frac{1}{1+\frac{1+\beta}{2}X}\frac{dE_0}{E_0} \tag{32}$$

for $\beta \to 1$ this result reproduces the second term of the right-hand side of Eq. (31).

We also derive the dependence of the outgoing photon energy spread on the energy spread of the incoming electron beam under the approximation of $\gamma \gg 1$, $\beta \simeq 1 - 1/2\gamma^2$:

$$\frac{dE'_0}{E'_0} = \frac{1}{1+\frac{1}{4\gamma^2}}\frac{2X + X^2 + X/\gamma}{X(1+X)}\frac{d\gamma}{\gamma} \tag{33}$$

This result reproduces the first term of the right-hand side of Eq. (31) at the limit $\gamma \gg 1$. So, in condition of large recoil, there is a sensible reduction of the bandwidth dependence on the electron beam emittance and the incident photon beam bandwidth, as already anticipated in Refs. [16,17]. This is well illustrated in Fig. 4, upper window, where our recent simulations confirm this effect firstly discovered and analyzed in Refs. [16,17]. In this figure, two different ways to produce 10 MeV radiation are presented: a scheme based on SCS, with 10 MeV electrons colliding with 10 MeV white spectrum photons (20% relative bandwidth) and, conversely (lower window), a conventional Inverse Compton Scattering source with parameters similar to ELI-NP-GBS (see [19,20]), with an electron beam of 659 MeV colliding with a laser pulse (1.5 eV photons) of 0.1% relative bandwidth. In the first case, the large recoil guarantees almost constant bandwidth with increasing emittance, the second one, characterized by small recoil factor, presents instead the typical bandwidth dependence on emittance introduced in Ref. [17], showing a crucial role of beam emittance in limiting the minimum bandwidth achievable in ICS. The two schemes exhibit advantages and drawbacks: while the first one is based on low energy, compact electron accelerators combined with broad-band gamma-ray sources (possibly represented by bremsstrahlung sources, or channeling radiation sources or radio-active sources), the second scheme adopts state-of-the-art lasers to produce the incident photon beams, but requires long and expensive GeV-class accelerators.

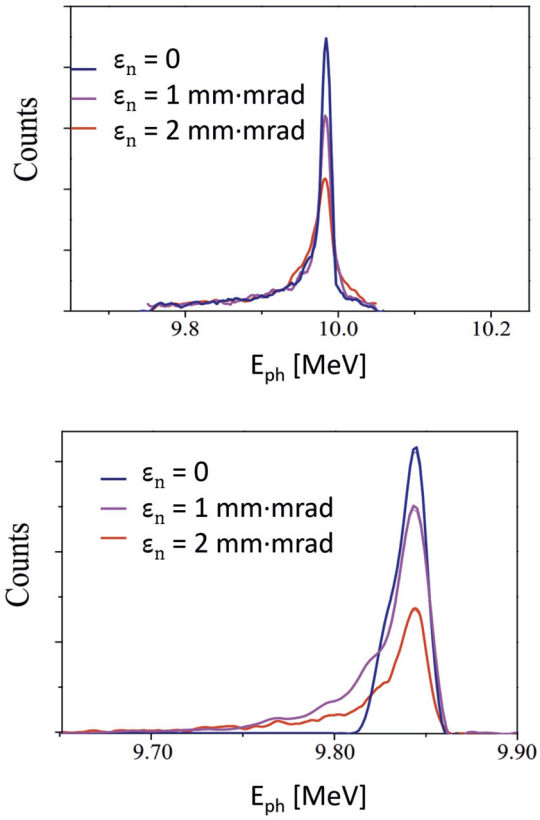

Fig. 4. Bandwidth dependence on electron beam emittance. Comparison between SCS and ICS. Upper window: electron energy 10 MeV, incident photon energy 10 MeV with 20% relative bandwidth, emitted photon energy 10 MeV, interaction rms spot size 10 μm, normalized emittance 0 mm·mrad,1 mm·mrad, 2 mm·mrad. Lower window: electron energy 659 MeV, incident photon energy 1.5 eV ($5 \cdot 10^{-4}$ relative bandwidth), collimation angle = 50 μrad, emitted photon energy about 10 MeV, interaction rms spot size 10 μm, normalized emittance 0 mm·mrad, 0.17 mm·mrad, 0.25 mm·mrad.

5. Symmetric Compton Scattering simulation

This chapter focuses on the Symmetric Compton Scattering simulations using two different codes to quantify the phenomenon. Unpolarized injected and emitted photons are considered. Our simulation approach investigates energy transfer, scattering angles and bandwidth variation of the particles that interacted.

5.1. WHIZARD

We used the WHIZARD code [21], a universal parton-level Monte Carlo event generator, to perform simulations of SCS.

An almost monochromatic (with an rms energy spread of the order of 10^{-4}) 10 MeV electron beam ($\beta \to 1$) collided head-on with an incoming photon beam characterized by large bandwidth (20% rms spread). The recoil in this interaction is large, the computed value being $X = 1533$. The results of the interaction, shown in Fig. 5, confirmed the theoretical predictions: the outgoing photons showed no correlation between energy and emission angle and featured a significant narrowing of the bandwidth ($2 \cdot 10^{-4}$ rms spread, i.e. a reduction of the energy spread by about 3 orders of magnitude from incident photon beam to the scattered photon beam). On the other hand, the electron beam emerging from the interaction inherited an high energy spread (of the order of 10^{-1}) from the original interacting photon beam, displaying an entropy exchange.

In order to qualitatively understand this effect of monochromatization we analyze, as an example, a very simple scenario of an electron propagating along the z-axis towards the right hand-side (positive component of its longitudinal momentum, vanishing transverse momentum) with energy 10 MeV and interacting with photons of a polichromatic beam. Three slightly different interactions with counter-propagating photons are considered: a) a 10 MeV photon (negative longitudinal momentum, vanishing transverse momentum) b) a 9 MeV photon a); and c) a 11 MeV momentum. The recoil parameter is 1533, 1379 and 1685, respectively. The center of mass reference system is steady in the lab frame system in case a), with exactly $\gamma_{cm} = 1$, while is moving with a speed $0.048c$ in case b) towards positive z (following the 10 MeV electron propagation) and $0.048c$ in case c) towards negative z (following the incident 11 MeV photon propagation). According to Eq. (15) due to the large values of the recoil parameter, the scattered photon will have an energy almost equal to the electron energy, i.e. 10 MeV, in all three cases. Since the motion of the center of mass system must be conserved, in case b) the scattered photon must be back-scattered and propagating along positive z, while the electron will be back-scattered

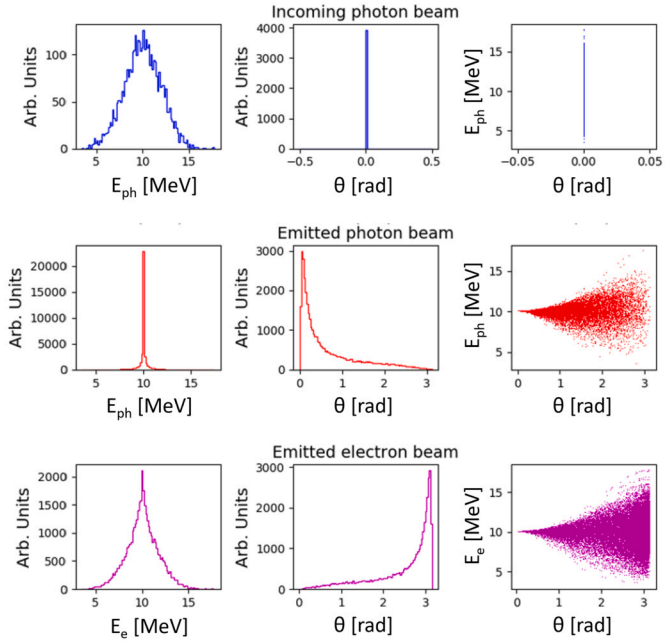

Fig. 5. Simulations of SCS. First row: incident photons. Second row: outgoing photons. Third row: and outgoing electrons. First column, energy distributions. Second column, angular distributions. Third column, energy vs angle θ. Average initial photon energy $\langle E_{\rm ph}\rangle = 10$ MeV, rms relative width of the distribution $\Delta E_{\rm ph}/E_{\rm ph} = 0.2$. Initial electron beams with average energy $\langle E_e\rangle = 10$ MeV and $\Delta E_e/E_e = 0$. Recoil factor: $X = 1533$.

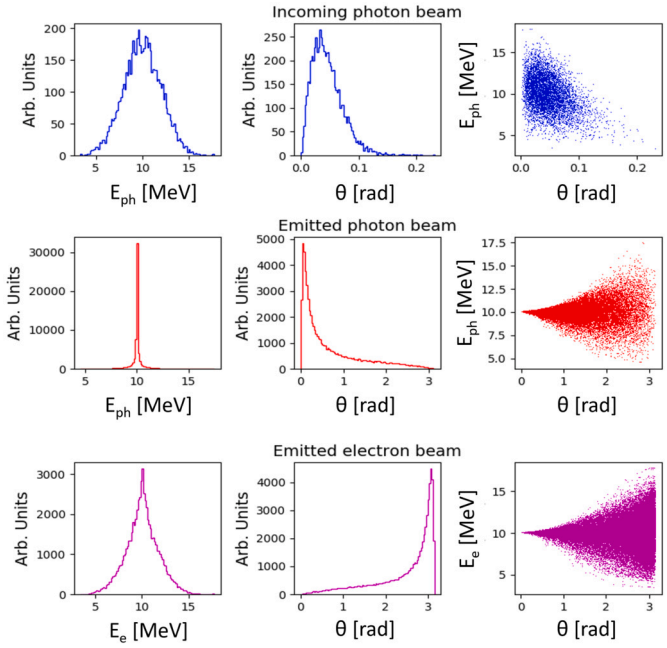

Fig. 6. Simulations of SCS. Plot arrangement similar to Fig. 5. Same parameters as Fig. 5, but adding an angular spread on the incoming photons. The distribution presents a slight correlation between angle of propagation and photon energy on the tail, removed in the interaction thanks to the high recoil factor ($X \sim 1533$).

and propagating along negative z with 9 MeV of energy. Similarly, in case c) the back-scattered photon will again propagate along positive z and the back-scattered electron towards negative z with 11 MeV energy. Therefore, scattered photons will pick up the monoenergetic 10 MeV electron energy, while electrons will be back-scattered with the energy of the incoming photons. Applying Eq. (1), we find that in case a) the back-scattered photon will have 9.98694 MeV energy, in case b) its energy will be 9.98622 and in case c) 9.98754. The total difference in scattered photon energy between case b) and case c) is 1.3 keV, while the energy difference between the incident photon energies is 2 MeV. Hence the strong cooling effect (more than 3 orders of magnitude) on the photon energy spread.

WHIZARD was also used to perform an analysis of the SCS effect in the presence of angular divergence of the incident photon beam, shown in Fig. 6, by mixing several runs with different incidence angles. The result confirms the SCS monochromatization also in one to one interactions characterized by small incidence angles.

5.2. Monte Carlo code

A home made multitasking Monte Carlo code has been developed, validated for different type of collisions and applied to the Compton scattering process [22]. As an additional internal feature, the code allows to consider the energy and angular (polar and azimuth) spread of both incident beams. To confirm the occurrence of the effect, we performed the same simulation of the deep recoil SCS interaction (at $X = 1533$) made with Whizard. Our findings confirm the exchange of entropy, resulting in a reduction of the bandwidth of the emitted radiation and an enlargement of the electron's bandwidth (as summarized in Fig. 7).

Furthermore, we examined the transition from the SCS regime to the ICS regime, with a particular focus on the angular distribution of the scattered radiation. To explore the transition regime, we started with the deep recoil SCS interaction ($X = 1533$) and slightly increased the energy of the incident electron bunch, while reducing the energy of the photon bunch. We investigated three cases, specifically with electron-photon energies of ($E_e \simeq E_{ph} = 10$ MeV), ($E_e = 11$ MeV, $E_{ph} = 9.08$ MeV), and ($E_e = 12$ MeV, $E_{ph} = 8.33$ MeV). The results, depicted in Fig. 8, show the distribution shifting from an uncorrelated energy-angle pattern to a more correlated one, resembling the typical "mustache" shaped curve observed in ICS experiments, typical of the well-known $(\gamma\theta)^2$ dependence shown in the denominator of Eq. (14).

6. Cooling down photons and heating up electrons

In previous chapters, we have seen how Symmetric Compton Scattering at large recoil can transfer monochromaticity from the beam of electrons to the beam of photons, in such a way that broad band incident photon beams are transformed into narrow band photon beams by the scattering. This mechanism can be considered sort of a photon cooling effect via SCS by monoenergetic electron beams (as clearly shown in Fig. 5 and 6, and theoretically explained by Eq. (32) and (33)). After collision, the electron beam is instead heated up to a larger energy spread. The electron energy angular distribution is peaked forward in case of large recoil, as illustrated in Fig. 6, 7 and 8 (note that the incident photon beam is directed towards $\theta = 0$, while the colliding electron beam is directed toward $\theta = \pi$): the reason is due to the angular cross section dependence, that is forward peaked when the recoil parameter X is large. On the other hand, if SCS takes place at low recoils the two scattered beams of photons and electrons are almost isotropically diffused over the entire solid angle. As far as the electron beam is concerned, this is an effective heating of its transverse emittance, furthermore, it is a complete transfer of its initial dominant longitudinal momentum into a cloud of electrons with prevalent transverse momentum. The part of electron beam undergoing scattering is blown all over the solid angle. This effect may be exploited to capture an electron beam inside a MB. Such an effect does not occur in ICS: indeed let's consider the difference between ICS and SCS from the point of view of the scattered electron transverse momentum distribution. Following Eq. (14), we can see that in ICS conditions the scattered photon energy at an angle $\theta = 1/\gamma$ (assumed to be small, since $\gamma \gg 1$ in ICS) is $E'_{\rm ph} = \frac{4\gamma^2 E_{\rm ph}}{(2+X)}$,

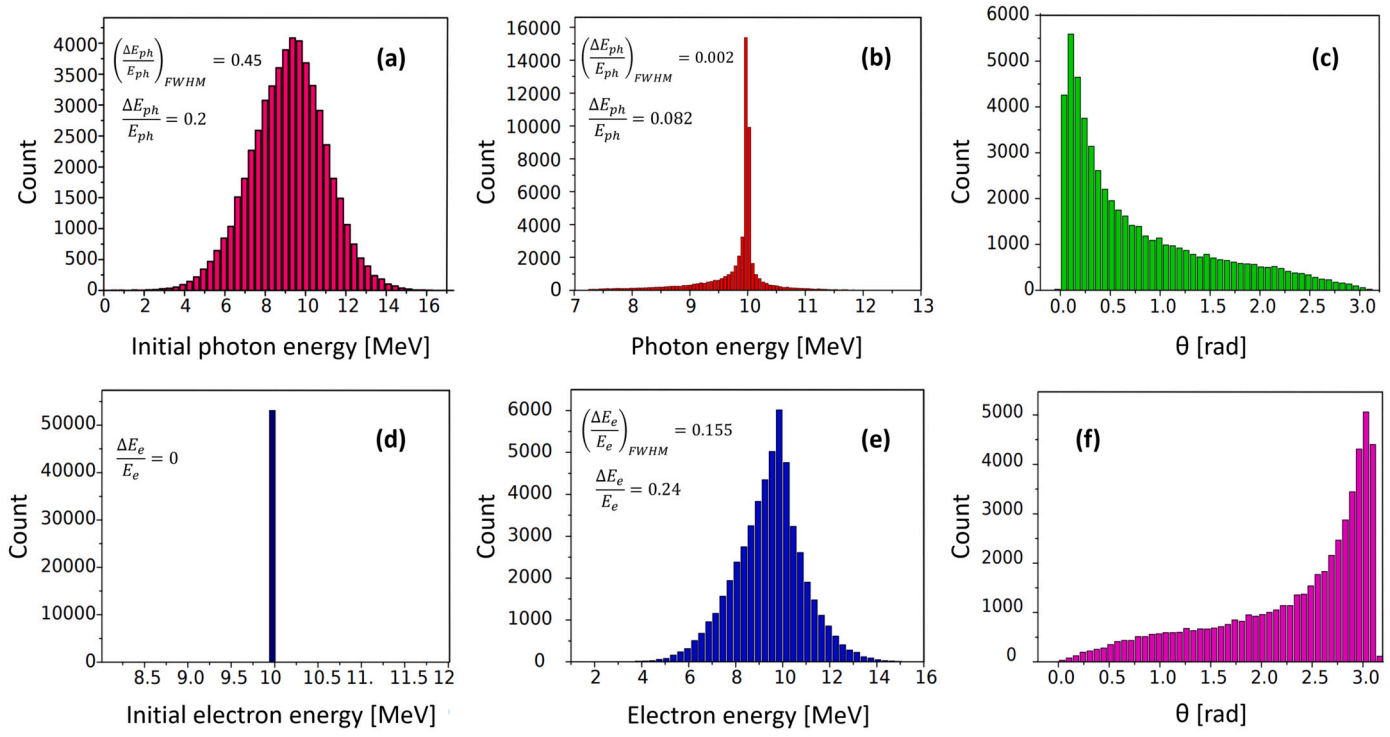

Fig. 7. Simulations of the SCS regime for a recoil factor of $X = 1533$. First row: photon beam. (a) Initial photon beams with average energy $\langle E_{\rm ph} \rangle = 10$ MeV and $\Delta E_{\rm ph}/E_{\rm ph} = 0.2$, (b) final photon energy with $\langle E_{\rm ph} \rangle = 10$ MeV and $\Delta E_{\rm ph}/E_{\rm ph} = 0.082$; (c) final angular photon distribution. Second row: electron beam. (d) Initial electron beams with average energy $\langle E_e \rangle = 10$ MeV and $\Delta E_e/E_e = 0$, (e) final electron distribution with $\langle E_e \rangle = 10$ MeV and $\Delta E_e/E_e = 0.155$; (f) final angular electron distribution.

therefore the associated transverse photon momentum is $p'_{\rm x-ph} = \frac{4\gamma E_{\rm ph}}{c(2+X)}$. Since the incident electron has a null transverse momentum before scattering, its transverse momentum after scattering will be $p'_{\rm x-e} = -p'_{\rm x-ph}$. Recalling the definition of the recoil factor X (Eq. (2)), we can derive an expression for the angle of scattering of the electron in ICS condition, i.e. $\theta'_e \simeq \frac{p'_{\rm x-e}}{p'_{\rm z-e}} \simeq \frac{X}{\gamma(2+X)}$. Therefore the scattered electrons in ICS are always propagating at small angles (and with small transverse momentum) around the axis of collision: the transfer of transverse momentum by the incident photon onto the scattered electron is almost negligible for all values of the recoil factor X. SCS at a low recoil factor is therefore the only mechanism to transfer large transverse momentum from the photon beam to the scattered electrons. A natural application of this mechanism would be the capture of an electron beam of suitable energy into a MB, transforming the beam into a plasma stored inside the bottle: this would be achieved by injecting the beam on-axis and colliding it with a beam of photons under SCS conditions.

As discussed above the scattered electrons would have a dominant transverse momentum and they would comply with the well known capture condition of a MB, i.e. $\frac{v_z}{v_r} < \sqrt{\frac{B_{\rm max}}{B_{\rm min}} - 1}$, where the radial velocity of a particle is $v_r = \sqrt{v_x^2 + v_y^2}$ [23]. We rewrite the capture condition as a function of the angle θ between the total velocity of the particle and the z-axis as:

$$|\tan\theta| > \left(\frac{B_{\rm max}}{B_{\rm min}} - 1\right)^{-\frac{1}{2}}. \tag{34}$$

To illustrate better this mechanism we take as an example a very simple conceptual setup of SCS performed at the center of a MB, between an injected electron beam of 5 keV kinetic energy and a counter propagating photon beam of 72 keV (so to comply with SCS condition stated by Eq. (16)). Given the low β of the electrons, the differential cross section is almost flat. The recoil factor is in this case small, i.e. $X = 0.57$.

The MB field map has been designed with Superfish [24], then imported in the Astra tracking code [25] to simulate the injection of the electron beam in the MB and imported in a tracking code made ad hoc to study the propagation of scattered electrons inside the MB. The on axis B_z field profile of the MB is shown in Fig. 9, with $B_{\rm max} = 2.3$ T and $B_{\rm min} = 0.9$ T. The capture condition for this MB is evaluated applying Eq. (34) so to find the minimum θ angle for a captured particle $\theta_{\rm min} = 0.674$ rad that translates to the following percentage of electrons emitted uniformly over the solid angle: $(\pi - 2\theta_{\rm min})/\pi \cdot 100 \sim 57\%$.

The control of the beam envelope during the injection into the MB along the symmetry axis requires a careful matching of the beam from the external region into the bottle, with the use of an additional solenoid lens to pre-focus the beam. As shown in Fig. 9, the beam achieves an equilibrium Brillouin flow inside the MB with almost 10 μm beam radius. Then, after propagating along the MB, while leaving the strong magnetic field region, the beam is strongly defocused.

The electrons undergoing a SCS collision in the inner region of the MB are spread all over the solid angle, converting their longitudinal momentum into transverse momentum. Fig. 10 shows the flat angular distribution (see discussion in Chapter 2 about the differential cross section) and the strong increase in the transverse momentum after the collision. Tracking the scattered electrons, we find that a large majority of them (60 over 100 tracked) are trapped in the MB, as clearly shown in Fig. 11. This result is in accordance with our predictions, considering the mild reduction of the emission distribution close to the z axis visible in Fig. 10 chart c) and the statistical error.

This clearly represents a possible mechanism of plasma heating by electrons trapped into the MB generated by a SCS interaction of the injected beam into the MB and a counter-propagating photon beam of equal momentum.

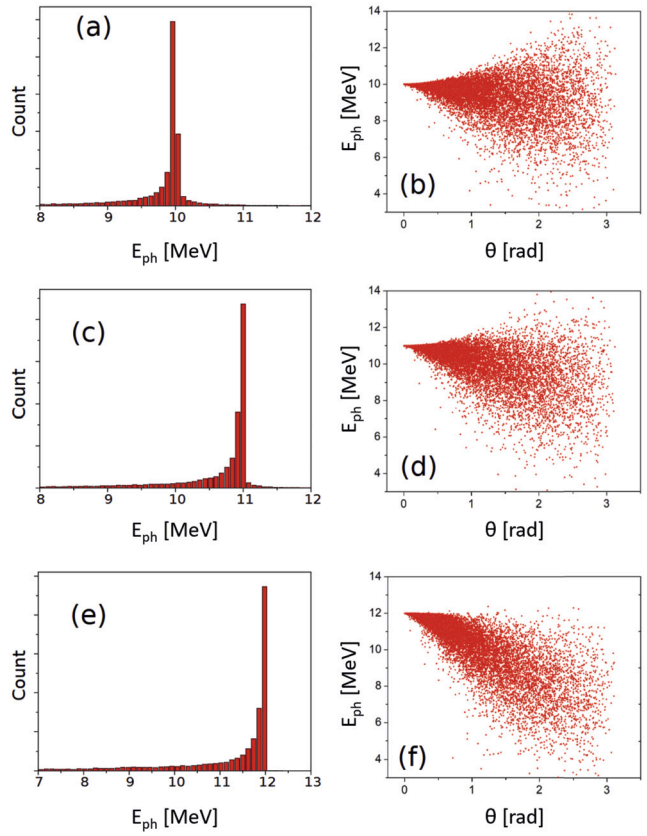

Fig. 8. This figure illustrates the regime transitions between SCS and ICS for three different sets of photons and electrons energy. (a) produced photon energy distribution and (b) angular photon distribution (i.e., energy as a function of emission angle) for an initial electron energy of 10.013 MeV and initial photon energy of 10 MeV. (c) Produced photon energy distribution and (d) angular photon distribution for initial electron energy of 11 MeV and initial photon energy of 9.08 MeV. (e) Produced photon energy distribution and (f) angular photon distribution for initial electron energy of 12 MeV and initial photon energy of 8.33 MeV.

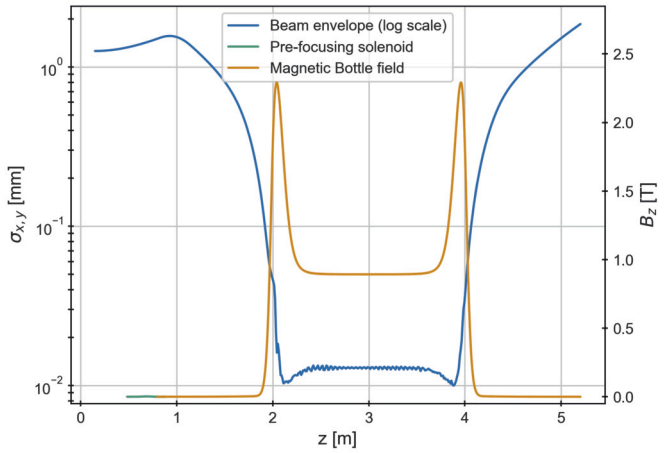

Fig. 9. This image shows the transverse envelope of the primary electron beam (in blue) before, during, and after propagation in the MB field (in gold the Bz field distribution). Before the bottle, the weak field (in green) of a solenoid, peaking at 2.5 mT, is visible and is used for matching into the bottle.

7. Conclusions

We explore the transition between Compton Scattering and Inverse Compton Scattering (ICS), a regime characterized by an equal exchange of energy and momentum between the colliding particles. This regime has been called Symmetric Compton Scattering (SCS) and has the unique property of transferring monochromaticity from one beam to the other, resulting in back-scattered photons that are intrinsically monochromatic. The paper suggests that large recoil SCS or quasi SCS can be used to design compact intrinsic monochromatic γ-ray sources, thus avoiding the use of GeV-class electron beams and powerful laser/optical systems typically required for ICS sources.

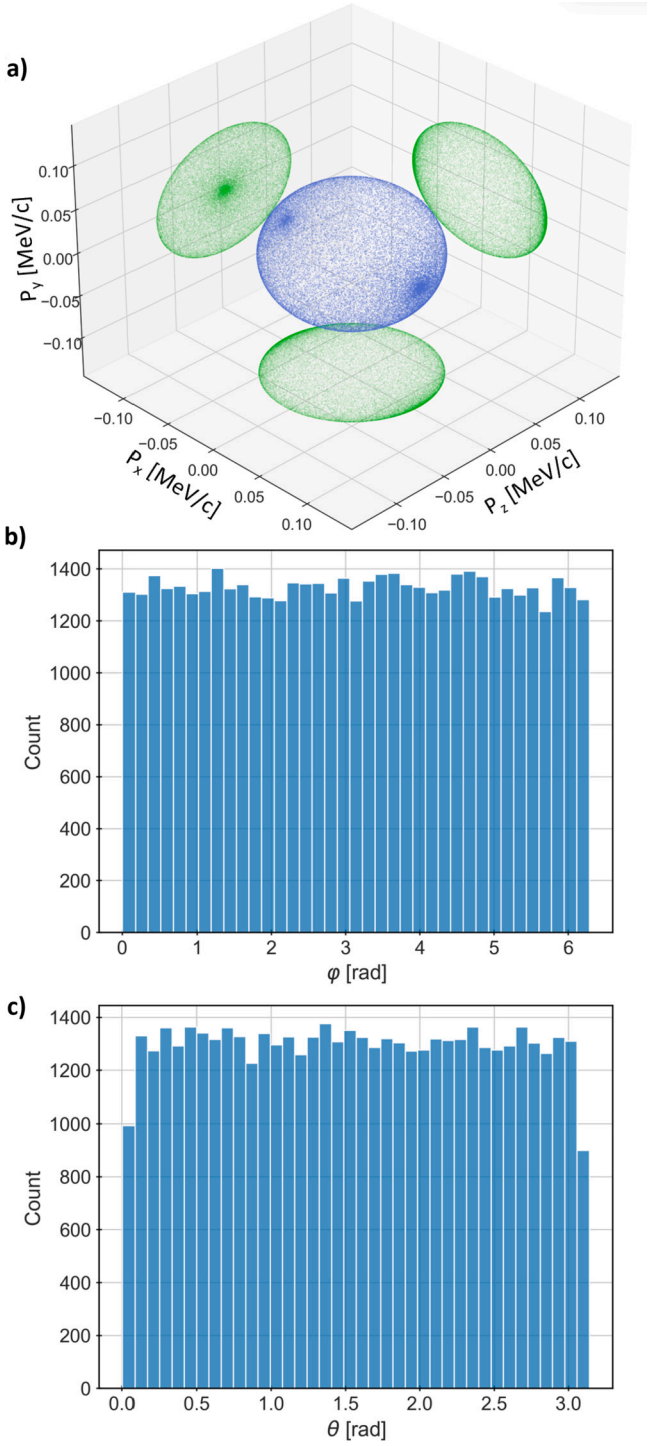

Fig. 10. Representation of the momenta of the electrons that interacted with the photons in SCS regime. a) 3D representation of the momenta with their projections. b) Distribution of the momenta respect the φ angle around the z-axis. c) Distribution of the momenta respect the θ angle with the z-axis.

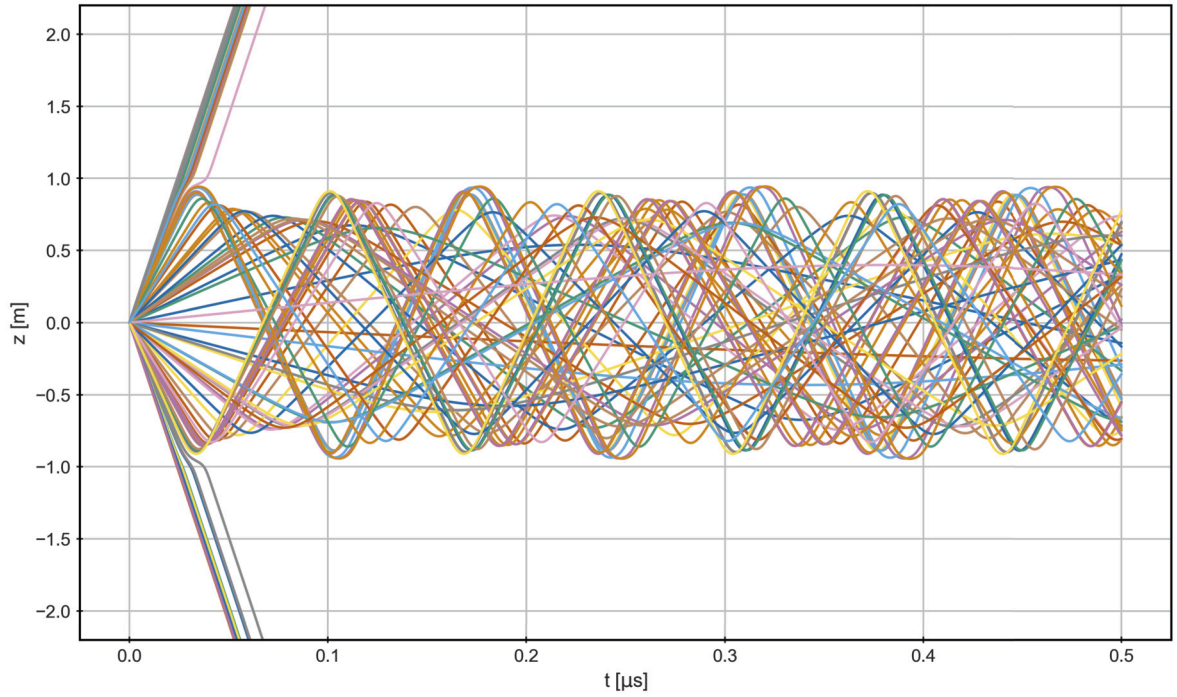

Fig. 11. Evolution of the longitudinal position of 100 particles tracked in the MB, 60% were trapped.

The capability of SCS regime to vanish the photon energy-angle correlation, married to the large recoil beneficial effects on the scattered photon energy spread, makes possible to conceive a monochromatic gamma ray beam source based on the collision between a bremsstrahlung radiation beam (or a coherent bremsstrahlung beam from a channeling source, [26]) and a monoenergetic electron beam of similar energy, say in the 2-10 MeV range. A compact source, developed on this concept, is much more sustainable than typical ICS sources for nuclear physics/photonics like ELI-NP-GBS [19], which envisages the use of GeV-class linear accelerators.

An Energy Recovery Linac with 10-20 MeV electron beam energy would allow sustaining a much larger average current (in the range of tens of mA) than a room temperature Linac like in ELI-NP-GBS, to the collision point with the broad band bremsstrahlung photon beam, compensating the decrease of total cross section σ with the recoil factor X typical of Klein-Nishina formula, as shown below (see Ref. [17])

$$\begin{cases} \lim_{X\to 0}\sigma = \dfrac{8\pi r_e^2}{3}(1-X) = \sigma_T(1-X) \\ \lim_{X\to\infty}\sigma = \dfrac{2\pi r_e^2}{X}\left(\log X + \dfrac{1}{2}\right) \end{cases} \tag{35}$$

A detailed study of a SCS γ-ray source will be the subject of future work, that will have to take into account the compensation of the cross section decrease for large recoils with the positive effects of reducing the photon bandwidth by large recoils, as shown by equations (31), (32) and (33) (assuming the capability to bring to collision a good quality electron beam with a small energy spread $\frac{\Delta_\gamma}{\gamma}$ below 10^{-3} [27]). The guidelines of such a design study should be oriented to optimize the SCS γ-ray source in terms of maximum Spectral Density S_d, as illustrated in Ref. [27] and typically requested by nuclear photonics and photo-nuclear physics applications. S_d is actually defined as $S_d \equiv N_{\rm ph}(\Delta E'_{ph}/E'_{ph})^{-1}$, where $N_{\rm ph}$ is the number of gamma ray photons generated per second within the relative bandwidth $\Delta E'_{ph}/E'_{ph}$ around the nominal average energy E'_{ph}. Since $N_{\rm ph}$ scales with the product $L\sigma$, where L is the collision luminosity and σ is given in Eq. (35), we see that for large recoil collisions S_d scales like $(L\log X)/X$. On the other side $\Delta E'_{ph}$ becomes very small in case of SCS at large recoil, as stated by equations (20), (32) and (33), and well illustrated in Fig. 5, 6 and 7, showing the potentiality of SCS to attain photon beams with relative bandwidths smaller than 10^{-3}.

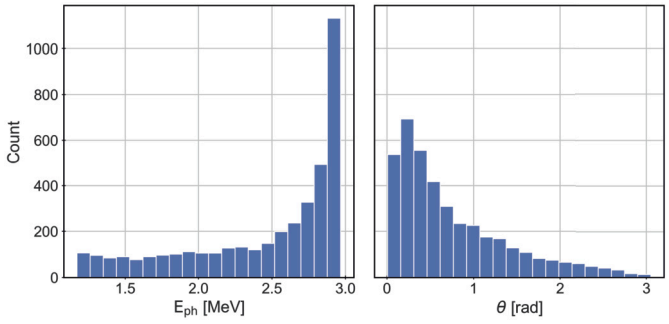

Fig. 12. Energy spectral distribution of scattered photons by a 3 MeV electron beam colliding with the photon beam of a $^{60}_{27}$Co radio-active source (left diagram). In the right diagram, the angular distribution is shown.

As a noticeable example of the application of SCS to nuclear photonics, we studied how to turn a fixed energy radioactive source of monochromatic γ-rays into a tunable source of monochromatic γ-ray photon beams. Assuming to take a photon beam emerging from a shielded and collimated Cobalt-60 ($^{60}_{27}$Co) radioactive source, with a double spectral line at 1.17 and at 1.33 MeV, we exploit the capability of quasi SCS at large recoil to scatter photons at an energy independent of the incident photon energy, but just equal to the incident electron energy, as illustrated above in Chapter 2 (see Eq. (15)). Colliding the γ-ray beam emerging from a $^{60}_{27}$Co source with a monoenergetic electron beam with 3 MeV energy (in this case the recoil factor $X = 54$), we find that the scattered photon will be spectrally peaked at 3 MeV with very narrow relative bandwidth, as shown below by the results of a Whizard simulation. The energy spectral distribution of scattered photons is shown in the left diagram of Fig. 12, while the angular distribution is in the right diagram. Most of the scattered photons have an energy close to 3 MeV (the incident electron energy) and are back-scattered close to $\theta = 0$, which is the direction of propagation of incident electrons. By se-

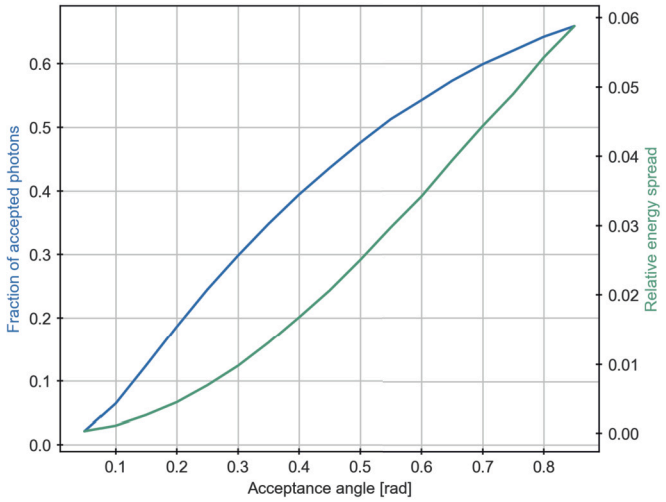

Fig. 13. Relative fraction of scattered photons within the acceptance angle (blue curve) and relative bandwidth of the selected photon beam within the angular acceptance (green curve).

lecting photons within a specific acceptance angle around $\theta = 0$ we can evaluate the fraction of selected photons and their relative bandwidth, as shown in Fig. 13. This example shows again a potential application in nuclear photonics exploiting the capability of SCS or quasi SCS to generate monochromatic gamma rays with compact low energy electron beams (i.e. MeV energy electrons instead of 100 MeV's). Symmetric Compton Scattering appears as a new modality of electron-photon interaction that holds promises to open new directions toward advanced radiation sources and plasma physics applications. The specific design of such radiation sources, as well as the expected performances in terms of achievable fluxes, or the detailed study of plasma confined systems based on SCS will be the subjects of future works.

CRediT authorship contribution statement

L. Serafini: Conceptualization, Formal analysis, Funding acquisition, Investigation, Project administration, Resources, Supervision, Validation, Writing – original draft, Writing – review & editing. **A. Bacci:** Formal analysis, Methodology, Software, Visualization, Writing – review & editing. **C. Curatolo:** Conceptualization, Formal analysis, Investigation, Methodology, Visualization, Writing – original draft, Writing – review & editing. **I. Drebot:** Methodology, Software, Writing – review & editing. **V. Petrillo:** Conceptualization, Formal analysis, Investigation, Methodology, Software, Supervision, Validation, Visualization, Writing – original draft, Writing – review & editing. **A. Puppin:** Methodology, Visualization, Writing – review & editing. **M. Rossetti Conti:** Formal analysis, Methodology, Software, Visualization, Writing – original draft, Writing – review & editing. **S. Samsam:** Writing – review & editing.

Declaration of competing interest

The authors declare that they have no known competing financial interests or personal relationships that could have appeared to influence the work reported in this paper.

Data availability

Data will be made available on request.

References

[1] A.H. Compton, A quantum theory of the scattering of x-rays by light elements, Phys. Rev. 21 (1923) 483–502, https://doi.org/10.1103/PhysRev.21.483.

[2] O. Kulikov, Y. Telnov, E. Filippov, M. Yakimenko, Compton effect on moving electrons, Phys. Lett. 13 (1964) 344–346, https://doi.org/10.1016/0031-9163(64)90040-X.

[3] L. Federici, G. Giordano, G. Matone, G. Pasquariello, P.G. Picozza, et al., Backward Compton scattering of laser light against high-energy electrons: the ladon photon beam at frascati, Il Nuovo Cimento B 59 (1980) 247–256, https://doi.org/10.1007/BF02721314.

[4] I.V. Pogorelski, I. Ben-Zvi, T.K.S. Hirose, et al., Demonstration of 8×10^{18} photons/second peaked at 1.8 a in a relativistic Thomson scattering experiment, Phys. Rev. Spec. Top., Accel. Beams 3 (2000).

[5] M. Bech, O. Bunk, C. David, R. Ruth, et al., Hard x-ray phase-contrast imaging with the compact light source based on inverse Compton x-rays, J. Synchrotron Radiat. 16 (2009) 43.

[6] K. Achterhold, K.M. Bech, S. Schleede, G. Potdevin, R. Ruth, R. Loewen, F. Pfeiffer, Monochromatic computed tomography with a compact laser-driven x-ray source, Sci. Rep. 3 (2013) 1313.

[7] C. Vaccarezza, D. Alesini, A. Anania, M.P. Bacci, A. Biagioni, F. Bisesto, M. Bellaveglia, P. Cardarelli, F.o. Cardelli, The sparc_lab Thomson source, Nucl. Instrum. Methods A 829 (2016) 237–242.

[8] W. Brown, S. Anderson, C. Barty, S. Betts, R. Booth, J. Crane, et al., Experimental characterization of an ultrafast Thomson scattering x-ray source with three-dimensional time and frequency-domain analysis, Phys. Rev. Spec. Top., Accel. Beams 7 (2004) 060702.

[9] H. Ikeura-Sekiguchi, R. Kuroda, M. Yasumoto, H. Toyokawa, M. Koike, K. Yamada, F. Sakai, K. Mori, K. Maruyama, H. Oka, T. Kimata, et al., In-line phase-contrast imaging of a biological specimen using a compact laser-Compton scattering-based x-ray source, Appl. Phys. Lett. 92 (2008) 131107.

[10] Y. Du, L. Yan, J. Hua, Q. Du, Z. Zhang, R. Li, H. Qian, W. Huang, H. Chen, C. Tang, Generation of first hard x-ray pulse at tsinghua Thomson scattering x-ray source, Rev. Sci. Instrum. 84 (2013) 053301.

[11] J. Kraemer, A. Jochmann, M. Budde, M. Bussmann, J. Couperus, T. Cowan, et al., Making spectral shape measurements in inverse Compton scattering a tool for advanced diagnostic applications, Sci. Rep. 8 (2018) 1398.

[12] N. Powers, I. Ghebregziabher, G. Golovin others, Quasi-monoenergetic and tunable x-rays from a laser-driven Compton light source, Nat. Photonics 8 (2014) 28–31.

[13] H.R. Weller, M.W. Ahmed, Y.K.o. Wu, Nuclear physics research at the high intensity gamma-ray source (hiγs), Nucl. Phys. News 25 (2015) 19–24.

[14] V. Petrillo, I. Drebot, M. Ruijter, S. Samsam, A. Bacci, C. Curatolo, M. Opromolla, M. Rossetti Conti, A. Rossi, L. Serafini, State of the art of high-flux Compton/Thomson x-rays sources, Appl. Sci. 13 (2023) 752, https://doi.org/10.3390/app13020752.

[15] P. Tomassini, A. Bacci, J. Cary, M. Ferrario, A. Giulietti, et al., Linear and nonlinear Thomson scattering for advanced x-ray sources in plasmonx, IEEE Trans. Plasma Sci. 36 (2008) 1782.

[16] R. Hajima, M. Fujiwara, Narrow-band gev photons generated from an x-ray free-electron laser oscillator, Phys. Rev. Accel. Beams 19 (2016) 020702.

[17] C. Curatolo, I. Drebot, V. Petrillo, L. Serafini, Analytical description of photon beam phase spaces in inverse Compton scattering sources, Phys. Rev. Accel. Beams 20 (2017) 080701, https://doi.org/10.1103/PhysRevAccelBeams.20.080701.

[18] N. Ranjan, B. Terzić, G.A. Krafft, V. Petrillo, I. Drebot, L. Serafini, Simulation of inverse Compton scattering and its implications on the scattered linewidth, Phys. Rev. Accel. Beams 21 (2018) 030701, https://doi.org/10.1103/PhysRevAccelBeams.21.030701.

[19] V. Petrillo, A. Bacci, C. Curatolo, I. Drebot, A. Giribono, C. Maroli, A.R. Rossi, L. Serafini, P. Tomassini, C. Vaccarezza, A. Variola, Polarization of x-gamma radiation produced by a Thomson and Compton inverse scattering, Phys. Rev. Spec. Top., Accel. Beams 11 (2015) 110701, https://doi.org/10.1103/PhysRevSTAB.11.110701.

[20] O. Adriani, et al., Technical design report eurogammas proposal for the eli-np gamma beam system, arXiv: Accelerator Physics, https://api.semanticscholar.org/CorpusID:119210258, 2014.

[21] W. Kilian, T. Ohl, J. Reuter, WHIZARD—simulating multi-particle processes at LHC and ILC, Eur. Phys. J. C 71 (2011) 1742, https://doi.org/10.1140/epjc/s10052-011-1742-y.

[22] C. Curatolo, High brilliance photon pulses interacting with relativistic electron and proton beams, Ph.D. thesis, University of Milan, 2022.

[23] J.D. Jackson, Classical Electrodynamics, 3rd ed., Wiley, New York, NY, 1999.

[24] M.T. Menzcl, H.K. Stokes, User's Guide for the POISSON/SUPERFISH Group of Codes, Accelerator Theory and Simulation Crmrp, AT-6, Los Alamos National Laboratory, Los Alamos, New Mexico 87545, 1987, L.A–UR–87–115 Issued: January 1987.

[25] K. Floettmann, Astra: a space charge tracking algorithm, http://www.desy.de/~mpyflo/, 1997.

[26] S.B. Dabagov, N.K. Zhevago, On radiation by relativistic electrons and positrons channeled in crystals, Riv. Nuovo Cimento 9 (2008) 491–530, https://doi.org/10.1393/ncr/i2008-10036-x.

[27] A. Bacci, D. Alesini, P. Antici, M. Bellaveglia, R. Boni, et al., Electron linac design to drive bright Compton back-scattering gamma-ray sources, J. Appl. Phys. 113 (2013) 194508, https://doi.org/10.1063/1.4805071.